RESEARCH ARTICLE | AUGUST 08 2022

Concurrence of auxetic effect and topological phase transition in a 2D phosphorous nitride ⊘

Jiangxin Liu; Chao Wu ⓘ ; Yuee Xie ✉ ; Xiaohong Yan; Qing Peng ✉ ; Yuanping Chen ✉ ⓘ

Check for updates

View Online

Export Citation

12 April 2024 07:47:47

Concurrence of auxetic effect and topological phase transition in a 2D phosphorous nitride

View Online   Export Citation   CrossMark

Jiangxin Liu,[1,2] Chao Wu,[1] Yuee Xie,[1,2,a] Xiaohong Yan,[1] Qing Peng,[3,a] and Yuanping Chen[1,a]

AFFILIATIONS

[1]School of Physics and Electronic Engineering, Jiangsu University, Zhenjiang 212013, Jiangsu, China
[2]School of Physics and Optoelectronics, Xiangtan University, Xiangtan, Hunan 411105, China
[3]State Key Laboratory of Nonlinear Mechanics, Institute of Mechanics, Chinese Academy of Sciences, Beijing 100190, China

[a]Authors to whom correspondence should be addressed: yueex@ujs.edu.cn; chenyp@xtu.edu.cn; and pengqing@imech.ac.cn

ABSTRACT

The auxetic effect and topological phase transition are interesting mechanical and electronic properties of some materials, respectively. Although each has been extensively studied separately, no material has been identified to possess both properties simultaneously. Here, we report that a two-dimensional phosphorous nitride monolayer simultaneously possesses auxetic behavior and undergoes a topological phase transition under tensile strain. The monolayer has a normal-auxeticity mechanical phase transition when a tensile strain above 0.055 is applied along the P–P zigzag direction. The negative Poisson ratio can even approach as abnormally high as -0.60. Furthermore, the material is an intrinsic Dirac material, but a phase transition from the semi-Dirac material to Dirac material is observed at nearly the same critical tensile strain as that in auxetic phase transition. An electronic orbital analysis reveals that the simultaneity of the normal-auxeticity phase transition and topological phase transition originates from the variation of orbital hybridization around the Fermi level.

The peculiar mechanical, thermal, electrical, optical, and other physical phenomena of materials continue to attract researchers to explore the mysteries and beauty of nature.[1,2] The auxetic effect is one of these peculiar mechanical phenomena.[3–6] Poisson's ratio (PR), a mechanical quantity, describes the negative ratio of transverse strain to longitudinal strain.[7] Most materials have a positive Poisson's ratio (PPR), which means that they undergo a transverse contraction (expansion) when stretched (compressed).[8] In contrast, some materials with negative Poisson's ratio (NPR), i.e., the so-called auxetic materials, expand laterally when stretched and contract laterally when compressed.[9–12] Auxetic materials can be classified into different categories. Some materials have an auxetic effect on several directions, while others only have the effect along one certain direction.[13] Some materials are half-auxetic because they exhibit auxetic phenomena only under a certain compressive or tensile strain.[14,15] Furthermore, some materials have transition of auxetic effect, i.e., when a critical strain is applied, they will experience a transition from a PPR to NPR.[16] Graphene is a type of material that belongs to the last category.[17] It transits from normal to auxetic phase when a tensile strain above 0.06 is applied along the armchair–chain direction. There is a magic angle (about 11° to the armchair direction) for auxeticity that, above this angle, the auxetic phase transition disappears.[18] In

nature, auxetic materials are quite rare compared to normal materials. However, their unusual mechanical behaviors have attracted significant attention owing to their unique properties for both fundamental research and potential applications in biomedicine,[19] fasteners, sensors,[20] national security,[21] defense,[22] and other fields.

Regarding electronic properties, topological phases and topological materials have been a focus of research for the past two decades.[23–25] Topological materials can be classified into three categories: topological insulator, topological semimetal, and topological metal.[26–28] Topological semimetals can be further divided into Dirac semimetal,[29–32] Weyl semimetal,[33,34] and nodal-line semimetal.[35,36] The topological phase transition can be induced by an external strain on a topological material.[37–39] For example, a two-dimensional (2D) semi-Dirac semimetal evolves into a Dirac semimetal when a tensile strain is applied to silicene oxide;[38] a nodal-line semimetal evolves into a Dirac/Weyl semimetal when a strain destroys the symmetry of the topological material.[40,41] These studies indicate that the electronic properties are strongly correlated with the mechanical properties. However, to date, there is no report on any material that possesses auxeticity and topological phase transition simultaneously.

Here, we investigate the mechanical and electronic properties of a monolayer phosphorous nitride (PN) made of zigzag chains.

The result shows that there exists an auxetic effect when a tensile strain above 0.055 is applied to the 2D structure along the P–P zigzag direction. The NPR can even approach −0.60. There is no auxetic effect when a compressive/tensile strain is applied in other directions. More interestingly, when the auxetic effect occurs, a topological phase transition from a semi-Dirac semimetal to a Dirac semimetal also occurs simultaneously. An analysis of variations of orbital hybridization under strains explains the changes in electronic and mechanical properties.

Density functional theory (DFT) first-principles calculations have been carried out using the Vienna *ab initio* simulation package (VASP).[42,43] Exchange correlation functionals are processed by the Generalized Gradient Approximation (GGA)[44] proposed by Perdew and Burke and Ernzerhof (PBE).[45] The projector-augmented plane wave (PAW) approach[46,47] is used to describe the ion–electron interaction. The plane wave cutoff energy is 600 eV. The convergence criterion of the force on each atom is 0.001 eV/Å. The energy convergence is achieved when the difference between two successive electronic energies is less than 1×10^{-6} eV. In order to eliminate an artificial layer–image interaction under periodic boundary conditions, a 20 Å vacuum layer is used in the z direction. The geometric optimization and self-consistent calculation of the initial structure are carried out by a $11 \times 13 \times 1$ Monkhorst Pack k-point grids. Under uniaxial loading, the stress–strain curves are calculated. The uniaxial strains along x and y are defined as $\varepsilon_x = (a - a_0)/a_0$, $\varepsilon_y = (b - b_0)/b_0$, respectively, where a_0 and b_0 are lattice constants free of strain, while a and b are lattice constants with strains. Strain–strain curves are fitted by a fourth-order polynomial. The PRs along x and y directions are computed by $-d\varepsilon_x/d\varepsilon_y$ and $-d\varepsilon_y/d\varepsilon_x$. To assess the lattice dynamical instability, the phonon dispersion curves are determined within the framework of the finite displacement method as implemented in the PHONOPY code.[48]

The atomic structure of monolayer PN is shown in Figs. 1(a) and 1(b). The 2D structure is made of zigzag chains along both x and y

directions. The P and N atoms form alternative zigzag chains along y the direction, while the P atoms form zigzag chains along the x direction, as shown in Fig. 1(b). The structural space group belongs to *Pmma* (D_{2h}^5). The primitive cell is shown in Fig. 1(c), where the lattice constants are labeled as a and b. The lengths of bonds N–P and P–P are labeled as l_1 and l_2, while the next-nearest-neighbor distances between the atoms in the zigzag chains along y and x directions are labeled as l_3 and l_4 [see Fig. 1(b)]. The thickness of the monolayer structure is labeled as d. After structural optimization, the structural parameters free of strain can be obtained. The lattice constants are $a_0 = 3.61$ and $b_0 = 2.73$ Å. The length of bonds N–P and P–P is $l_{10} = 1.61$ and $l_{20} = 2.29$ Å, respectively. The next-nearest-neighbor distance between the atoms in the zigzag chains along y and x directions is $l_{30} = 2.73$ and $l_{40} = 3.61$ Å, respectively. The thickness of the monolayer structure is $d_0 = 3.12$ Å.

We have first calculated the elastic constants of the monolayer structure. Our results are $C_{11} = 54.05$, $C_{12} = 7.09$, $C_{22} = 268.54$, and $C_{66} = 23.71$ N/m. They satisfy the Born stability criterion for an orthorhombic system: $C_{11} > 0$, $C_{22} > 0$, $C_{66} > 0$, and $C_{11} + C_{22} - 2C_{12} > 0$. According to these quantities, the Young's modulus Y and shear modulus G can be obtained. The in-plane Young's modulus along x and y axes is $Y_x = 53.86$ and $Y_y = 267.61$ N/m, respectively. The shear modulus is $G = 23.71$ N/m. These results indicate that the 2D material possesses good flexibility and strong anisotropic mechanical properties. We also calculate the stability of the structure under strains. The results are shown in Fig. S1 in the supplementary material. The monolayer structure is stable when the uniaxial strains ε_x and ε_y are in the ranges (−0.05, 0.17) and (−0.05, 0.23), respectively.

We then explore mechanical responses of the 2D material to the applied uniaxial strains. When a uniaxial strain ε_x is applied along x axis, the corresponding variations of structural parameters l_1, l_2, l_3, and l_4 are shown in Fig. 2(a). The length l_2 of bond P–P and the next-nearest-neighbor distance l_4 between P atoms change linearly with the strain rapidly. This is because the bonds P–P extend along the
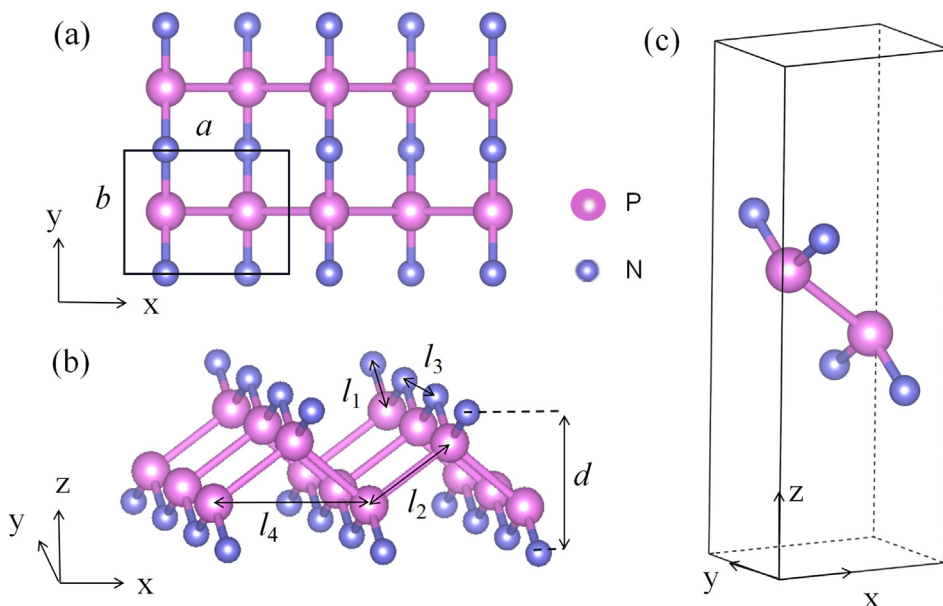
FIG. 1. Atomic structure of monolayer PN on the top view (a) and side view (b), where the purple and blue spheres represent P and N atoms, respectively. The lattice constants are labeled as a and b in (a). The lengths of bonds N–P and P–P are labeled as l_1 and l_2 in (c), while the next-nearest-neighbor distances between the atoms in the zigzag chains along y and x directions are labeled as l_3 and l_4, respectively. The thickness of the monolayer structure is labeled as d. (c) A primitive cell of the PN structure.

FIG. 2. (a) The variations of bond lengths l_1, l_2 and atomic next-nearest-neighbor distances l_3 and l_4 with respect to a uniaxial strain ε_x. (b) The variations of resultant strain ε_y and PR as a function of a uniaxial strain ε_x. No NPR is found. (c) The variations of bond lengths l_1, l_2 and atomic next-nearest-neighbor distances l_3 and 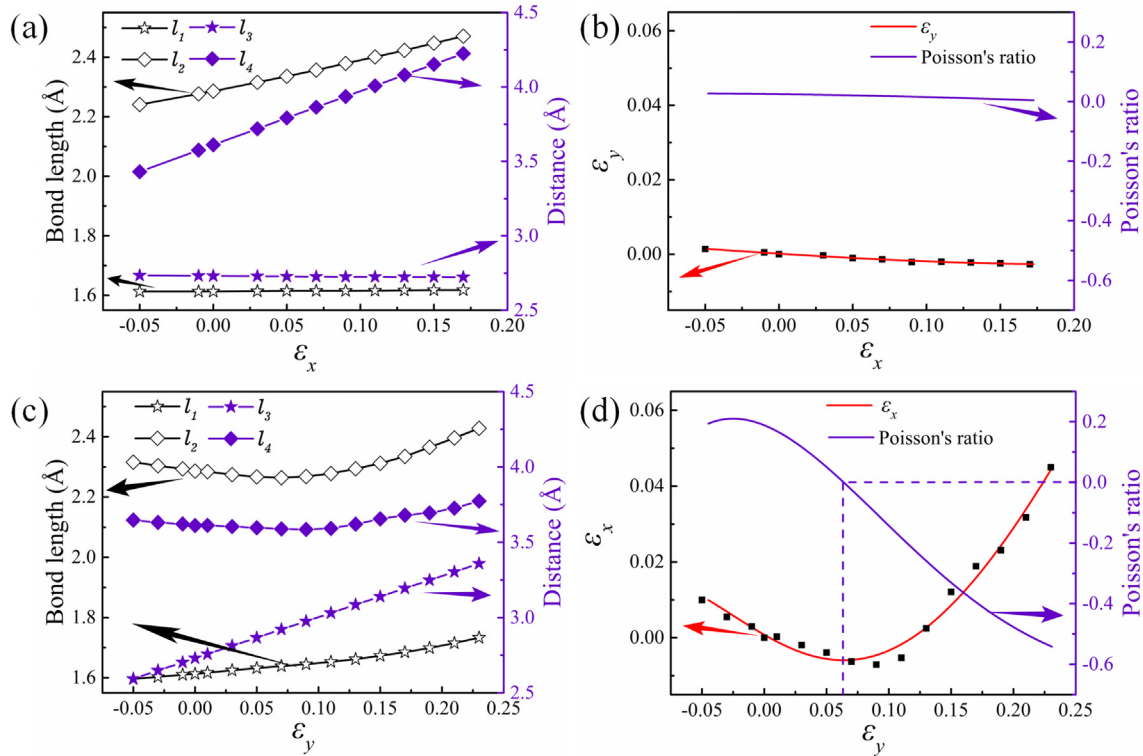l_4 in response to a uniaxial strain ε_y. (d) The variations of resultant strain ε_x and PR with a uniaxial strain ε_y. NPR is found after $\varepsilon_y > 0.55$.

x direction. Thus, a tensile strain ($\varepsilon_x > 0$) results in l_2 and l_4 increasing while a compressive strain results in decreasing. However, the two lengths l_1 and l_3 seem insensitive to the strain ε_x. It indicates that the strain along x direction nearly has no effect on the bonds P–N along the y direction. Figure 2(b) presents resultant strain ε_y along the y direction with the variation of the applied strain ε_x. This further illustrates that the effect of applied strain ε_x on structural deformation along the y direction is very weak, because ε_y is close to zero. As a result, the Poisson's ratio is nearly equal to zero.

Figure 2(c) shows the variations of structural parameters when a uniaxial strain ε_y is applied along the y direction. To accommodate the strain, the length l_1 of bond P–N and l_3 monotonically changes with ε_y, because the bond P–N extends along the y direction. Different from Fig. 2(a), the strain ε_y causes significant changes of l_2 and l_4, i.e., the strain along the y direction leads to substantial structural deformation along the x direction. Moreover, the variations of l_2 and l_4 are non-monotonic. In the case of a compressive strain along the y direction ($\varepsilon_y < 0$), l_2 and l_4 increase with the strength of the strain. This is a normal mechanical response of a material with PPR. In the case of a tensile strain along the y direction ($\varepsilon_y > 0$), l_2 and l_4 decrease first and then increase with ε_y. The transition point is around $\varepsilon_y = 0.055$. This indicates that, when $\varepsilon_y > 0.055$, a tensile strain results in the structure expanding in the perpendicular direction, i.e., auxeticity. To clearly show the auxeticity, Fig. 2(d) shows ε_x and PR with the variation of ε_y. The variation of ε_x is a U-shaped curve, and the minimum value is at

the point $\varepsilon_y = 0.055$. The PR is negative when $\varepsilon_y > 0.055$. The NPR value can be as abnormally large as -0.60 (60%). The stress–strain curves and the changes in total energy with strains are given in Figs. S2(a) and S2(b) in the supplementary material, respectively.

In addition, we investigate the mechanical response of the structural thickness d. The variations of d under a uniaxial strain ε_x and ε_y are displayed in Fig. S2(c) in supplementary material, respectively. No auxetic effect is found according to the variations of the curves.

The monolayer PN is an intrinsic Dirac material.[49] Figure 3(a) shows its orbital projected band structure in the strain-free status. Along Γ-Y, there is a Dirac point D_1 on the spectrum. The location of the Dirac point in the first Brillouin zone (BZ) is illustrated in Fig. 3(d). Another Dirac point D_2 is a symmetry point of D_1 because of the time reversal symmetry. Therefore, the structure is a Dirac material with two Dirac points.

To study the coupling of the auxeticity and topological phase transition, we calculate variation of electronic properties of the structure under ε_y. We find that the two bands which named B_1 and B_2 around the Fermi level along Γ-Y become closer with an increase in a tensile strain ε_y. When the value ε_y is around 0.055, the two bands contact together and then a crossing point Q_1 is formed, as shown in Fig. 3(b). As mentioned below, Q_1 is a semi-Dirac point rather than a Dirac point. The original Dirac points D_1 and D_2 are insensitive to the strain. As a result, there are two Dirac points D_1 and D_2 on the k_y axis and two semi-Dirac points Q_1 and Q_2 on the k_x axis in the first BZ
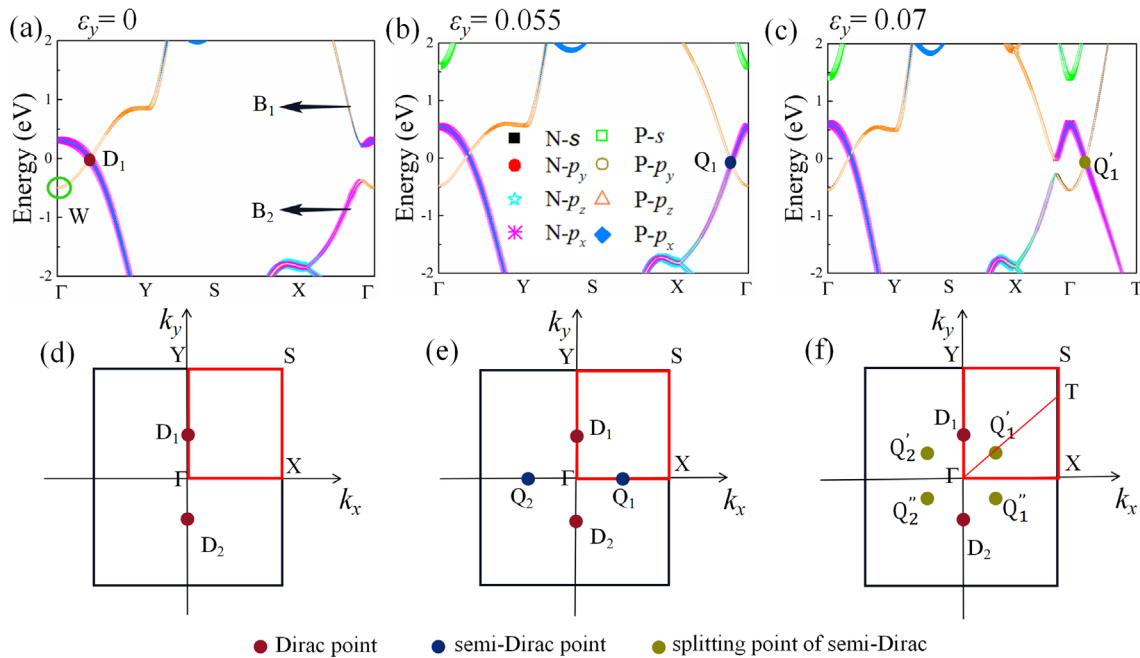
FIG. 3. The orbital projected band structures of monolayer PN under a uniaxial strain (a) $\varepsilon_y = 0$, (b) $\varepsilon_y = 0.055$, and (c) $\varepsilon_y = 0.07$. (d)–(f) The topological phases in the first BZ corresponding to the band structures in (a)–(c), respectively.

[see Fig. 3(e)]. As seen from Figs. 3(a) and 3(b), the orbital projected bands illustrate the evolution of band inversion.

With a further increase in ε_y, say $\varepsilon_y = 0.07$, the two bands around the Fermi level along Γ-Y separate again, as shown in Fig. 3(c). A detailed calculation indicates that the semi-Dirac points split to four Dirac points. For example, Q_1 splits to Q_1' and Q_1''. Q_1' locates on the k path Γ-T in Fig. 3(f). Their corresponding energy bands are given in Fig. 3(c). As a result, there are six Dirac points in the first BZ, whose topological phase is shown in Fig. 3(f). Therefore, the uniaxial strain ε_y along y axis induces a topological phase transition from two Dirac points to six Dirac points. The critical phase is a topological semimetal with two Dirac points and two semi-Dirac points. Moreover, the critical strain is nearly equal to that of the auxetic effect. The coincidence of the phase transform of auxeticity and topological phase at the same strain implies that they might have the same origin.

To clearly illustrate the topological phases in Fig. 3, we present energy bands around the Dirac points D_1 and Q_1' and semi-Dirac point Q_1, as shown in Figs. 4(a)–4(c), respectively. As seen from Fig. 4(a), the point D_1 is crossed by linear bands along both k_x and k_y directions and, thus, is a Dirac point. The three-dimensional (3D) energy bands in Fig. 4(d) around the point D_1 further illustrate that it is a standard Dirac point. As shown in Fig. 4(b), the point Q_1 is crossed by two linear bands along k_x and by two quadratic bands along k_y, i.e., Q_1 is a semi-Dirac point. Its 3D energy bands are given in Fig. 4(e). The evolution between Dirac points and semi-Dirac points is somewhat similar to the Ref. 38. The energy bands in Fig. 4(c) and its 3D energy bands in Fig. 4(f) illustrate that Q_1' is a standard Dirac point.

The variation of the electronic properties of the monolayer PN under a uniaxial strain ε_x is shown in Fig. S3 in the supplementary material. The results indicate that the uniaxial strain ε_x has no effect

on the topological phase. The monolayer structure is always a Dirac material with two Dirac points on the k_y axis.

The above results demonstrate that a uniaxial strain induces an auxetic effect and topological phase transition simultaneously when $\varepsilon_y > 0.055$. What is the origin of the phenomenon? To answer this question, we have examined the variation of projected density of states (PDOS) with respect to the applied strain. Figures 5(a)–5(d) and 5(e)–5(h) show the PDOS of N and P atoms varying with the uniaxial strain ε_y, respectively. One can find that the PDOS of P atoms has been significantly changed by the strain. For example, at $\varepsilon_y = 0$, the electronic states of P atoms below the Fermi level are dominated by p_z orbitals. With the variation of the strain, the ratio of s orbitals increases. At $\varepsilon_y = 0.11$, the electronic states below the Fermi level are dominated by s, p_x, and p_z orbitals, whose corresponding band structure is given in Fig. S4 in the supplementary material. This indicates that there is a significant variation of orbital hybridization of P atoms. The orbital hybridization above the Fermi level is also significantly changed by the strain. The variation of the orbital hybridization leads to the increase in the P–P bond length. As a result, the auxetic effect occurs.

To further explain the effect of strain ε_y on hybridization of orbitals, in Fig. S5 in the supplementary material, the variations of wavefunctions for quantum state at point W in Fig. 3(a) are examined. The wavefunctions of the P atoms are considerably changed by the strain. In the strain-free case, there are bonding states between the two nearest-neighbor P atoms. In the case of $\varepsilon_y = 0.11$, the bonding wavefunctions disappear because of the variation of the orbital hybridization, instead the next-nearest-neighbor P atoms form weak bonding states. Because the next-nearest-neighbor interactions are weaker than that of nearest-neighbor interactions, the length of bonds P–P
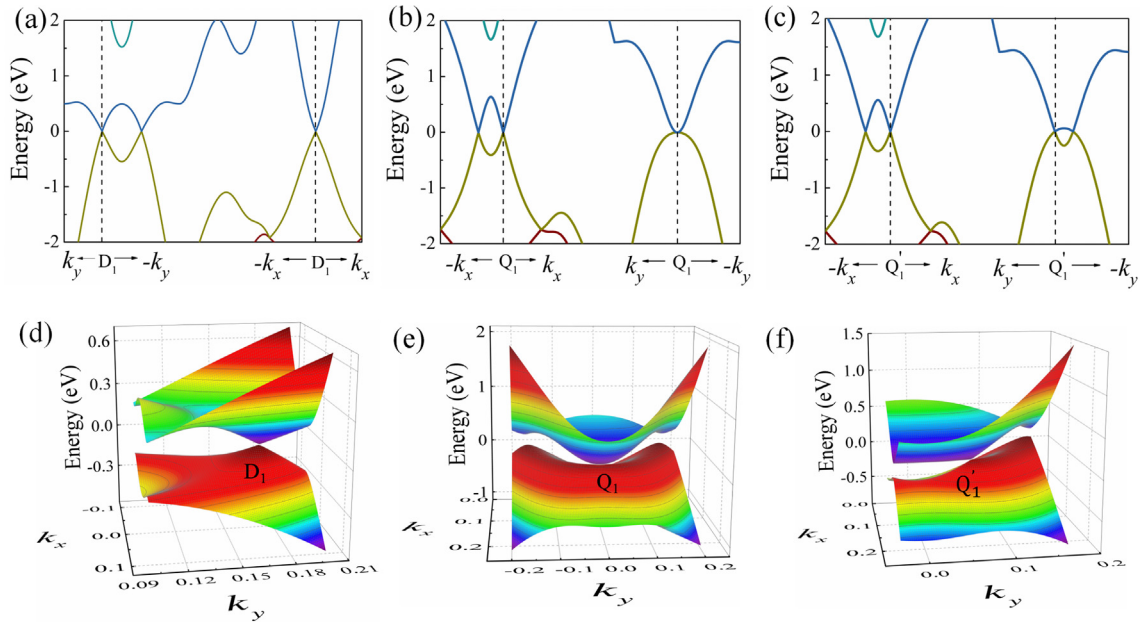
FIG. 4. Band structures around (a) the Dirac points D_1 in Fig. 3(a), (b) the semi-Dirac point Q_1 in Fig. 3(b), and (c) splitting Dirac point Q'_1 in Fig. 3(c) along directions parallel k_x or k_y in momentum space. (d)–(f) 3D energy bands around the points D_1, Q_1, and Q'_1 in (a)–(c), respectively.

increases rather than decreases. It is worth noting that the tensile strain ε_y is applied along the y direction, the strain extends not only P–N bonds along the y direction but also P–P bonds along the x direction. Therefore, the strain ε_y changes atomic orbital hybridization. On the

one hand, the energies of electronic states are changed, resulting in band crossings and topological phase transition; on the other hand, the mechanical interactions between atoms are also changed, resulting in an auxetic effect.
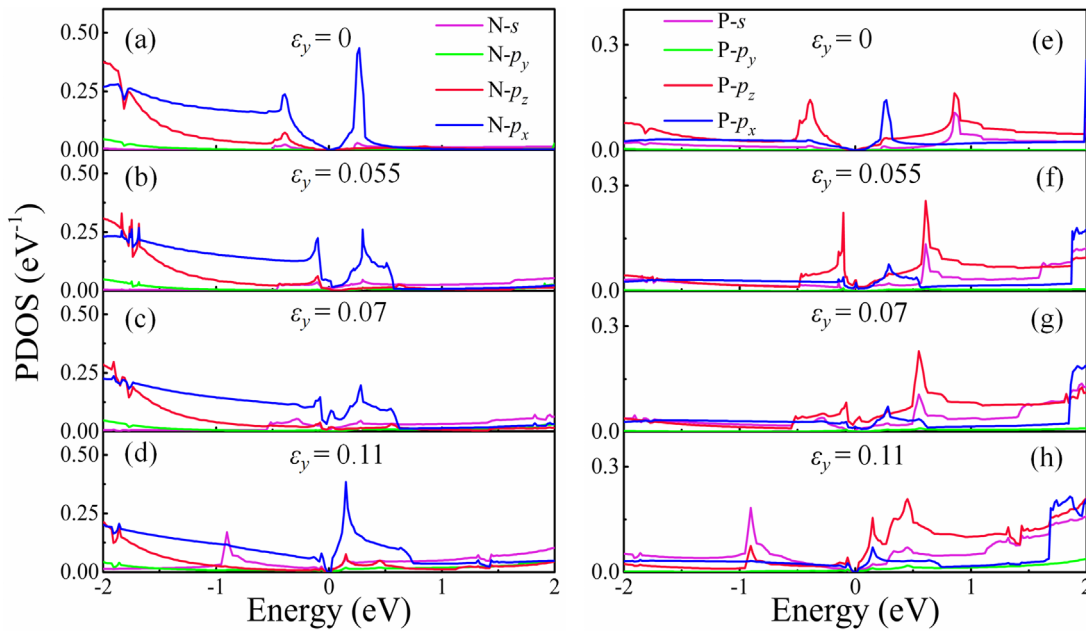

FIG. 5. The projected density of states (PDOS) of N atoms in the monolayer PN when a strain (a) $\varepsilon_y = 0$, (b) $\varepsilon_y = 0.055$, (c) $\varepsilon_y = 0.07$, and (d) $\varepsilon_y = 0.11$ is applied. The PDOS of P atoms in the monolayer PN when a strain (e) $\varepsilon_y = 0$, (f) $\varepsilon_y = 0.055$, (g) $\varepsilon_y = 0.07$, and (h) $\varepsilon_y = 0.11$ is applied.

In conclusion, we have investigated the mechanical and electronic properties of a monolayer PN made of zigzag chains. Both normal-auxetic phase and topological phase transitions occur when a tensile strain above 0.055 is applied on the 2D structure along the P–P zigzag direction. The value of NPR can even approach -0.60, which could be the highest record reported to date. There is no auxeticity when a compressive/tensile strain is applied in other directions. It is interesting that when the auxetic effect occurs, a topological phase transition from a semi-Dirac semimetal to a Dirac semimetal also occurs simultaneously. The coincidence of the phase transform of auxeticity and topological phase at the same strain implies that they have the same origin: the strain along the y direction changes the hybridization of atoms and then changes energies of the quantum states as well as the mechanical interactions between atoms. Our work not only has identified a material having both auxetic behavior and a topological phase transition, but also provides atomic insight on the origin and correlations between the two unique phase transitions.

See the supplementary material for phonon spectra, stress–strain curves, total energy of monolayer PN under different strains, variation of atomic layer thickness d with strains, electronic properties under a uniaxial strain, and wavefunctions under a uniaxial strain along the y-axis.

AUTHOR DECLARATIONS
Conflict of Interest
The authors have no conflicts to disclose.

Author Contributions
Jiangxin Liu: Writing – original draft (equal). **Chao Wu:** Writing – original draft (equal). **Yuee Xie:** Formal analysis (equal); Writing – original draft (lead). **Xiaohong Yan:** Conceptualization (equal); Writing – review editing (supporting). **Qing Peng:** Conceptualization (equal); Formal analysis (equal). **Yuanping Chen:** Funding acquisition (lead); Project administration (lead); Supervision (lead); Writing – review editing (lead).

DATA AVAILABILITY
The data that support the findings of this study are available within the article and its supplementary material.

REFERENCES
[1] Y. Du, J. Maassen, W. Wu, Z. Luo, X. Xu, and P. D. Ye, Nano Lett. **16**(10), 6701–6708 (2016).
[2] S. Sun, F. Meng, Y. Xu, J. He, Y. Ni, and H. Wang, J. Mater. Chem. A **7**(13), 7791–7799 (2019).
[3] G. Liu, Q. Zeng, P. Zhu, R. Quhe, and P. Lu, Comput. Mater. Sci. **160**, 309–314 (2019).
[4] Y. Wang, F. Li, Y. Li, and Z. Chen, Nat. Commun. **7**(1), 11488 (2016).
[5] S. Guo and H. Sun, Phys. Rev. B **102**(18), 184116 (2020).
[6] Q. Wei, Y. Yang, A. Gavrilov, and X. Peng, Phys. Chem. Chem. Phys. **23**(7), 4353–4364 (2021).
[7] D. Wu, S. Wang, S. Zhang, J. Yuan, B. Yang, and H. Chen, Phys. Chem. Chem. Phys. **20**(28), 18924–18930 (2018).
[8] Q. Wei and X. Peng, Appl. Phys. Lett. **104**(25), 251915 (2014).
[9] Y. Li, S. Wang, and B. Yang, ACS Omega **6**(23), 14896–14902 (2021).
[10] M. Sun and U. Schwingenschlögl, J. Phys. Chem. C **125**(7), 4133–4138 (2021).
[11] B. Wang, Q. Wu, Y. Zhang, L. Ma, and J. Wang, ACS Appl. Mater. Interfaces **11**(36), 33231–33237 (2019).
[12] J. N. Grima, S. Winczewski, L. Mizzi, M. C. Grech, R. Cauchi, R. Gatt, D. Attard, K. W. Wojciechowski, and J. Rybicki, Adv. Mater. **27**(8), 1455–1459 (2015).
[13] J.-W. Jiang and H. S. Park, Nat. Commun. **5**(1), 4727 (2014).
[14] F. Ma, Y. Jiao, W. Wu, Y. Liu, S. A. Yang, and T. Heine, Nano Lett. **21**(6), 2356–2362 (2021).
[15] Z. Gao, Q. Wang, W. Wu, Z. Tian, Y. Liu, F. Ma, Y. Jiao, and S. A. Yang, Phys. Rev. B **104**(24), 245423 (2021).
[16] K. Bertoldi, P. M. Reis, S. Willshaw, and T. Mullin, Adv. Mater. **22**, 361–366 (2010).
[17] B. Deng, J. Hou, H. Zhu, S. Liu, E. Liu, Y. Shi, and Q. Peng, 2D Mater. **4**(2), 021020 (2017).
[18] J. Hou, B. Deng, H. Zhu, Y. Lan, Y. Shi, S. De, L. Liu, P. Chakraborty, F. Gao, and Q. Peng, Carbon **149**, 350–354 (2019).
[19] F. Scarpa, IEEE Signal Process. Mag. **25**, 128–126 (2008).
[20] Y. Jiang, Z. Liu, N. Matsuhisa, D. Qi, W. R. Leow, H. Yang, J. Yu, G. Chen, Y. Liu, C. Wan, Z. Liu, and X. Chen, Adv. Mater. **30**(12), e1706589 (2018).
[21] P. U. Kelkar, H. S. Kim, K. H. Cho, J. Y. Kwak, C.-Y. Kang, and H. C. Song, Sensors **20**, 3132 (2020).
[22] K. K. Saxena, R. Das, and E. P. Calius, Adv. Eng. Mater. **18**(11), 1847–1870 (2016).
[23] P. Liu, J. R. Williams, and J. J. Cha, Nat. Rev. Mater. **4**(7), 479–496 (2019).
[24] B. Yan and C. Felser, Annu. Rev. Condens. Matter Phys. **8**(1), 337–354 (2017).
[25] L. Xie, H. Wu, L. Jin, and Z. Song, Phys. Rev. B **104**(16), 165422 (2021).
[26] B.-J. Yang and Y. B. Kim, Phys. Rev. B **82**(8), 085111 (2010).
[27] X.-L. Qi and S.-C. Zhang, Rev. Mod. Phys. **83**(4), 1057 (2011).
[28] X. Wan, A. M. Turner, A. Vishwanath, and S. Y. Savrasov, Phys. Rev. B **83**(20), 205101 (2011).
[29] A. Narayan, Phys. Rev. B **91**, 205445 (2015).
[30] L.-Y. Feng, R. A. B. Villaos, A. B. Maghirang, Z.-Q. Huang, C.-H. Hsu, H. Lin, and F.-C. Chuang, Sci. Rep. **12**(1), 4582 (2022).
[31] S. M. Young and C. L. Kane, Phys. Rev. Lett. **115**(12), 126803 (2015).
[32] S. M. Young, S. Zaheer, J. C. Teo, C. L. Kane, E. J. Mele, and A. M. Rappe, Phys. Rev. Lett. **108**(14), 140405 (2012).
[33] S. Jia, S.-Y. Xu, and M. Z. Hasan, Nat. Mater. **15**(11), 1140–1144 (2016).
[34] M. Naher and S. Naqib, Sci. Rep. **11**(1), 5592 (2021).
[35] H. Zhang, Y. Xie, Z. Zhang, C. Zhong, Y. Li, Z. Chen, and Y. Chen, J. Phys. Chem. Lett. **8**(8), 1707–1713 (2017).
[36] J. He, X. Kong, W. Wang, and S.-P. Kou, New J. Phys. **20**(5), 053019 (2018).
[37] C. Lin, M. Ochi, R. Noguchi, K. Kuroda, M. Sakoda, A. Nomura, M. Tsubota, P. Zhang, C. Bareille, K. Kurokawa, Y. Arai, K. Kawaguchi, H. Tanaka, K. Yaji, A. Harasawa, M. Hashimoto, D. Lu, S. Shin, R. Arita, S. Tanda, and T. Kondo, Nat. Mater. **20**(8), 1093–1099 (2021).
[38] C. Zhong, Y. Chen, Y. Xie, Y.-Y. Sun, and S. Zhang, Phys. Chem. Chem. Phys. **19**(5), 3820–3825 (2017).
[39] Z. Wu, Z. Shen, Y. Xue, and C. Song, Phys. Rev. Mater. **6**(1), 014011 (2022).
[40] Y. Du, F. Tang, D. Wang, L. Sheng, E.-J. Kan, C.-G. Duan, S. Y. Savrasov, and X. Wan, npj Quantum Mater. **2**(1), 3 (2017).
[41] J. Li, H. Wang, and H. Pan, Phys. Rev. B **104**(23), 235136 (2021).
[42] J. Hafner, J. Comput. Chem. **29**(13), 2044–2078 (2008).
[43] G. Kresse and J. Furthmüller, Phys. Rev. B **54**(16), 11169–11186 (1996).
[44] J. P. Perdew and W. Yue, Phys. Rev. B **33**(12), 8800–8802 (1986).
[45] J. P. Perdew, K. Burke, and M. Ernzerhof, Phys. Rev. Lett. **77**(18), 3865–3868 (1996).
[46] N. A. W. Holzwarth, G. E. Matthews, R. B. Dunning, A. R. Tackett, and Y. Zeng, Phys. Rev. B **55**(4), 2005–2017 (1997).
[47] P. E. Blöchl, Phys. Rev. B **50**(24), 17953–17979 (1994).
[48] A. Togo and I. Tanaka, Scr. Mater. **108**, 1–5 (2015).
[49] Y. Xie, Y. Kang, S. Li, X. Yan, and Y. Chen, Appl. Phys. Lett. **118**, 193101 (2021).